FABRICATION OF PVDF/PES NANOFIBERS WITH UNSMOOTH FRACTAL SURFACES BY ELECTROSPINNING
A General Strategy and Formation Mechanism

by

Ling LIN*[a], *Yan-Qing LIU*[b], *Yun-Yu LI*[c], *Yue SHEN*[d], and *Ji-Huan HE*[b,e]

[a] Zhejiang Fashion Institute of Technology, Ningbo, China
[b] National Engineering Laboratory for Modern Silk, College of Textile and Clothing Engineering, Soochow University, Suzhou, China
[c] School of Textile Science and Engineering, Xi'an Polytechnic University, Xi`an, China
[d] School of Science, Xi'an University of Architecture and Technology, Xi'an, China
[e] School of Mathematics and Information Science, Henan Polytechnic University, Jiaozuo, China

Original scientific paper
https://doi.org/10.2298/TSCI191201024L

Smaller fibers are welcome in many applications due to larger surface area, but there is a threshold for smallest fibers for a fixed spinning system. In order to further improve surface area, hierarchical structure is considered in this paper using electrospinning. A bi-solvent system is used in our experiment for fast solvent evaporation. Unsmooth nanofibers are obtained, and the formation mechanism is elucidated.

Key words: *electrospinning, sudden solvent evaporation, surface energy, geometric potential, hierarchical structure*

Introduction

It becomes a trend to improve specific surface area in many areas, such as nanotechnology, material science, chemistry, tissue engineering, energy science and textile engineering. A higher specific surface area means a higher surface energy (surface potential), which can result in more fascinating properties and more attractive applications [1-8].

Nanofibers have extremely high specific surface area, for example nanofibers with radius of 100 nm have ten thousand times higher surface area than that for a fiber with radius of 1mm, unsmooth surface can further improve 150%.

Hierarchical structure in nature always behaves extremely well in many aspects, for examples, the wool fiber hierarchy has excellent thermal property [9, 10], the polar bear hairs have remarkable thermal insulation property [11, 12], silkworm cocoon hierarchy has good air/water permeation and heat-proof property [13]. The hierarchical structure also enables Fuzhu, an ancient Chinese device, to collect water from air [14], and a nanofiber membrane or a filter with hierarchical structure always has good air permeability and low pressure drop [15-18].

Though there are many reports for producing unsmooth fibers [19, 20], its mechanism is not clear yet, furthermore the mechanism for attracting properties due to unsmooth surface with hierarchical structure is still an open problem. This paper gives a general strategy and formation mechanism for fabrication of hierarchical fibers.

* Corresponding author, e-mail: Hejihuan@suda.edu.cn

Surface energy (geometric potential) *vs.* surface area

Most chemical properties, mechanical properties and electronic properties are relative to the surface energy, or the geometric potential [21-29]. Any surface can produce a boundary-induced potential, for example, the gravity of the Earth [30]. It is simple way to improve the specific surface area by making material small, the smaller, the better. To illustrate the fact, we consider a fiber with length of L and radius of R, its surface area is $2\pi RL$ If the fiber is cut into N smaller daughter fibers with radius of r, the total surface area becomes $2\pi rLN$. According to the volume conservation (mass conservation), the fiber number can be calculated:

$$N = \frac{\pi R^2 L}{\pi r^2 L} = \frac{R^2}{r^2} \tag{1}$$

The surface area increases:

$$\frac{2\pi rLN}{2\pi RL} = \frac{R}{r} \tag{2}$$

Consider a spider silk with diameter of 3 μm, which is actually a nanofiber assembly consisting of nanofibers with diameters of about 20 nm. The surface area of the nanofiber assembly of the natural silk increases 150 times:

$$\frac{R}{r} = \frac{3\cdot 10^{-6}}{20\cdot 10^{-9}} = 150 \tag{3}$$

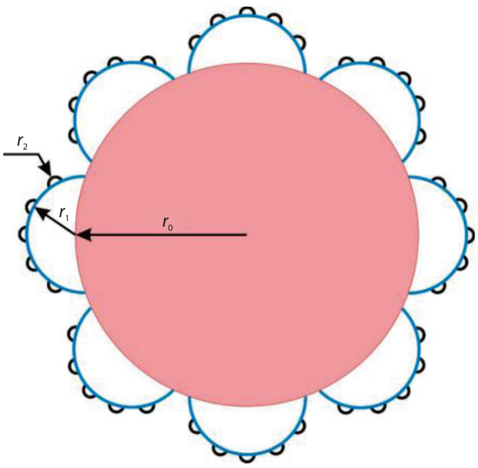

Figure 1. Fractal surface roughness

Unsmooth surface is a simple way to further improve surface area. Consider a fiber surfce on which hemispheres with radius of r are uniformly distributed, fig. 1, it can be easily calculated that the surface area increases about π/2 times comparfwith its smooth fiber.

The surface area can be only used for qualitative analysis, the most important factor is the surface energy or geometrical potential. For a sphere the geometrical potential can be written [21, 30]:

$$E \propto \frac{1}{r} \tag{4}$$

where r is the radius of the sphere. The potential can produce a force:

$$F = \frac{\partial E}{\partial r} \propto -\frac{1}{r^2} \tag{5}$$

Equation (4) implies a smaller sphere can produce a higher geometrical potential or a larger force. The well-known stress concentration is a good example for explanation of eq. (5): a sudden change of geometrical structure will produce a sharp stress concentration, which will become weaker if a more smooth surface is formed. To further illustrate this fact, we consider a simple case in fig. 1: r_0 =1000 nm, r_1 = 100 nm, and r_2 = 1 nm, as a result each hierarchical cascade has the potential:

$$E_1 = \frac{r_0}{r_1} E_0 = 10 E_0 \tag{6}$$

and

$$E_2 = \frac{r_0}{r_2} E_0 = 1000 E_0 \tag{7}$$

In practical applications, we always use average sradius of the unsmooth surface for example, for the hierarchical structure given in fig. 1, if we use r_1 as its average radius, r_2 is sothing of square deviation. If the average radius is used, eq. (4) has to be updated:

$$E \propto \frac{1}{r_1^\alpha} \tag{8}$$

where α is a scaling exponent, for the illustrating example, $\alpha = 3$:

$$\frac{E_{\text{average}}}{E_0} = \left(\frac{r_0}{r_{\text{average}}}\right)^3 = \left(\frac{1000}{100}\right)^3 = 1000 \tag{9}$$

In a summary, when r tends nanoscales, eq. (4) should be updated:

$$E \propto \frac{1}{r^\alpha} \tag{10}$$

where r is the average radius, α is a scaling exponent. eq. (10) can explain the Hall-Petch effect in material science [31]. When r tends to a molecular scale, the value of the scaling exponent can be as large as 12 as that for the Lennard-Jones potential [32].

The nanoeffect can be written [33]:

$$\sigma = \sigma_0 \left(1 + \frac{k}{r^{3/2}}\right) \tag{11}$$

where σ is the can be elastic modulus or strength, σ_0 – the its bulk's property, k – the material constant, and r – the fiber's radius.

In this paper we will suggest a simple way to produce rough surface by electrospinning.

Theoretical development

Electrospinning is generally used to produce smooth micro/nanofibers, but unsmooth fiber with hierarchical structure can be produced by adjusing spinning parameters [33-35]. Figure 2 is a control volume for the moving jet during the spinning process, the mass lose due to the solvent evaporation can be calculated using the Darcy law:

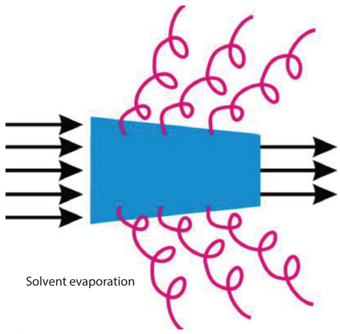

Figure 2. A control volume of a moving jet in the spinning process

$$Q_{\text{evaporation}} = 2\pi r \rho_s V = 2\pi r \rho_s k \nabla p = 2\pi r \rho_s k (p - p_0) \tag{12}$$

where V is the evaporation velocity, ρ_s – the solvent's density, Δp – the pressure difference between the jet surface and the atmospheric pressure, and k – the constant.

The mass conservation equation considering the solvent evaporation can be expressed:

$$\pi r^2 \rho u + Q_{\text{evaporation}} = \pi r^2 \rho u + 2\pi r \rho_s k (p - p_0) = Q \tag{13}$$

where u is the velocity of the jet, ρ – the density of the jet, r – the radius of the jet, and Q – the flow ratio which is a constant in our study.

We assume that the moving jet follows Bernoulli's principle:

$$\frac{1}{2}u^2+\frac{p}{\rho}=B \tag{14}$$

where B is the Bernoulli constant. By eq. (14), we can re-write eq. (13):

$$\pi r^2\rho u+2\pi r\rho_s k\left(\rho B-\frac{1}{2}\rho u^2-p_0\right)=Q \tag{15}$$

The jet radius can be solved from eq. (15):

$$r=\frac{-2\pi\rho_s k\left(b-\frac{1}{2}\rho u^2\right)+\sqrt{\left[2\pi r\rho_s k\left(b-\frac{1}{2}\rho u^2\right)\right]^2+4\pi\rho uQ}}{2\pi\rho u} \tag{16}$$

where $b=\rho B-p_0$.

It is not very difficult to find:

$$\frac{\mathrm{d}r}{\mathrm{d}u}=-\frac{r^2\rho-2r\rho_s k\rho u}{2r\rho u+2\rho_s k\left(b-\frac{1}{2}\rho u^2\right)} \tag{17}$$

Generally a higher voltage results in a higher acceleration, as a result, a higher velocity is obtained, and a smaller fiber is predicted. However, there is a critical value for the jet radius:

$$r_{cr}=2\rho_s ku \tag{18}$$

When $r>r_{cr}$, we have $\mathrm{d}r/\mathrm{d}u<0$, it implies an increase of velocity results in decrease of jet radius. However, when a fast solvent evaporation occurs, k is large in eq. (18), the jet radius will sooner reach its critical value, when $r<r_{cr}$, we have $\mathrm{d}r/\mathrm{d}u>0$, that means the jet radius will increase when the jet velocity increases, however, this will not happen, because during the spinning process, solidification of the jet begins at the very initial stage, the section area cannot be enlarged for a solidifying jet, that means when the jet radius reaches $r=r_{cr}$ the jet radius will keep almost unchanged, while the solvent evaporation still continues, resulting in unsmooth surface. The general strategy for fabrication of unsmooth fibers by electrospinning is to control the critical radius given in eq. (18), the two key factors for this purpose are solvent evaporation ratiom, k, and jet velocity, u, we will give an experimental verification of our theoretical prediction.

Experimental design

In order to give an experimental verification of the aforementioned theoretical analysis, we used dimethyl formamide (DMF) and acetone as solvents. Acetone is a volatile solvent with w boiling point of 56 °C, and the boiling point is lower for the bi-solvent system.

In our experiment, polyvinylidene fluoride (PVDF), and poly(ether sulfones) (PES) were used without any purification, which were bought from, respectively, 3M Company, US and American Solvay.

A bi-solvent system was first prepared with a weight ratio: DMF/acetone = 7/3. The PVDF powders were put into the bi-solvent system in a sealed beaker, the mixture was then magnetically stirred using a magnetic stirrer (DF-101S, Xinrui Instrument Co. Ltd.) with the water temperature of 50 °C until a uniform and transparent solution was obtained. The PES particles were then put into the PVDF solution, and the mixture was stirred using a magnetic stirrer

(HJ-6A,Gongyi Yuhua Instrument Co. Ltd.) under ambient temperature until a uniform and transparent solution was formed. Concentrations of PVDF/PES solution were listed in tab. 1.

Table 1. The PVDF/PES solution

PVDF [g]	PES [g]	DMF [g]	Acetone [g]	Concentration [%]
1.5	1.5	11.9	5.1	15
2	2	12.32	5.28	20

Electrospinning was used in this paper to prepare for unsmooth nanofibers. The PVDF/PES solution was put into a 10 mL syringe, other parameters were listed in tab. 2.

Table 2. Spinning parameters

Samples	Voltage [Kv]	Receptor distance [cm]	Rate of solution supply [mLh^{-1}]	PVDF/PES concentration [%]	Average diameter [nm]
1	15	17	0.5	15	431±24.18
2	17	17	0.5	15	508±24.15
3	20	17	0.5	15	587±30.33
4	15	17	1	20	836±80.00

Results and discussion

The SEM illustrations for each sample are given in figs. 3 and 4, average fiber diameter for each sample is listed in tab. 2.

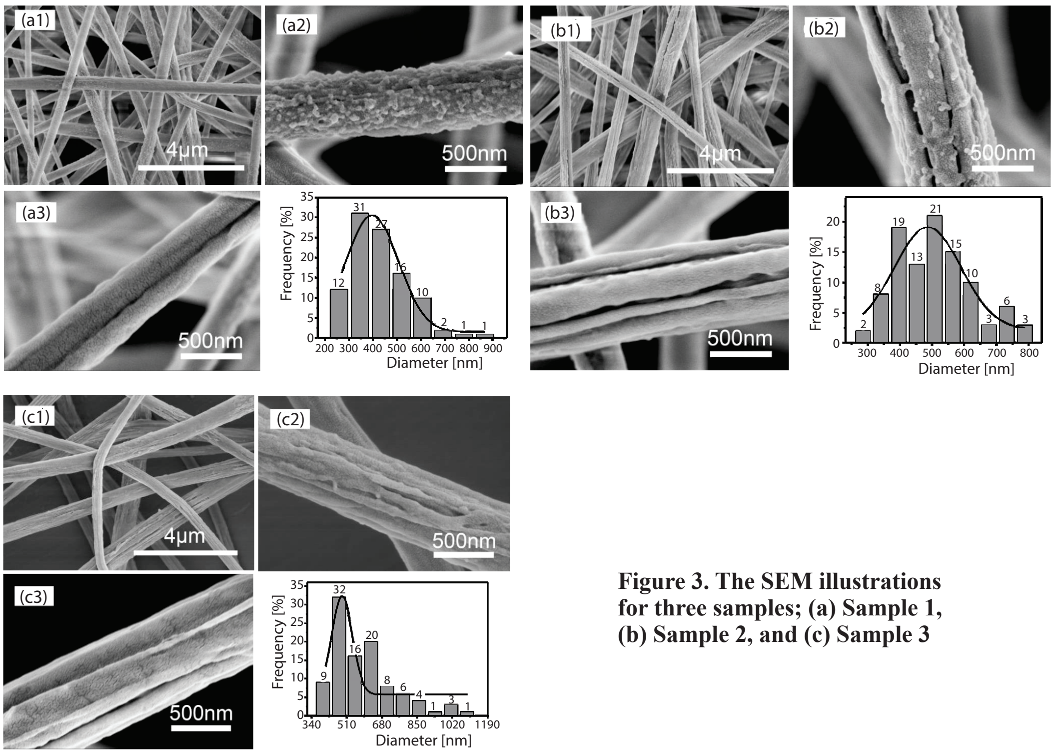

Figure 3. The SEM illustrations for three samples; (a) Sample 1, (b) Sample 2, and (c) Sample 3

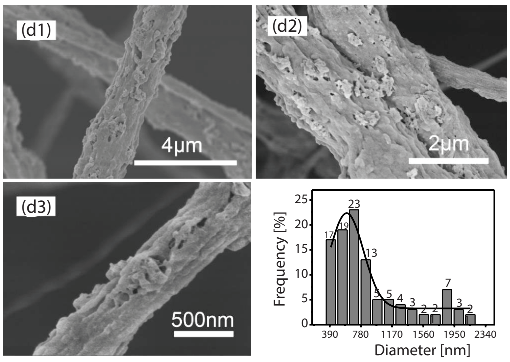

Figure 4. The SEM illustrations for Sample 4

Figure 3 shows that a lower voltage results in smaller fibers with more unsmooth surface. This is because a lower voltage implies a lower acting force, as a result a slower velocity of the jet is predicted due to lower acceleration, according to eq. (18), the critical radius is smaller than those for Samples 2 and 3, this result agrees with the experimental observation given in figs. 1-3 and tab. 2.

We assume that the jet's velocity is proportional to the applied voltage:

$$E \propto u \tag{19}$$

The final fiber radius is determined by the critical radius given in eq. (18):

$$r_{cr} \propto E \tag{20}$$

Using the data given in tab. 2:

$$\frac{(r_{cr})_1}{(r_{cr})_2} = \frac{E_1}{E_2} = \frac{15}{17} = 0.88 \tag{21}$$

and

$$\frac{(r_{cr})_1}{(r_{cr})_3} = \frac{E_1}{E_3} = \frac{15}{20} = 0.75 \tag{22}$$

While the observed results are, respectively, 431/508 = 0.848 and 431/587 = 0.734, this simple theoretical analysis gives a high accuracy of predictions, 3.8% and 2.1%, respectively.

As the distance between the needle and the receptor was fixed in our experiment, a lower velocity of the jet means a long exposure period for solvent evaporation, resulting in unsmooth surface. For a faster moving jet, according to Bernoulli principle, the surface pressure of the moving jet is lower, resulting in a lower pressure difference between the jet surface and its atmosphere pressure, according to Darcy law, the solvent evaporation is slower, as a result, a more smooth surface is predicted as the cases for Samples 2 and 3.

The jet velocity mainly depends upon the applied voltage, but there is another very important factor which was always ignored in academic community, that is the supply rate of the spun solution. The solution supply rate of Sample 4 is twice as those for other three samples.

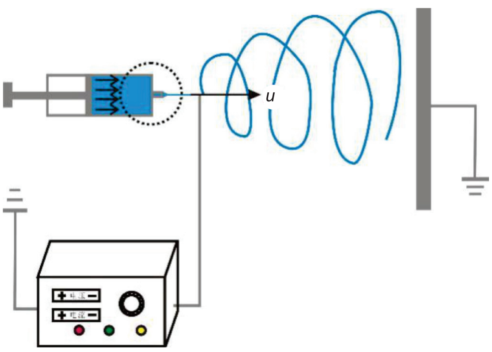

Figure 5. A control volume (discontinuous circle)

Figure 5 gives a control volume for mass conservation, for a steady spinning process, the mass entering into the control volume equals to the mass discharging:

$$\pi r_0^2 \rho u_0 = Q \tag{23}$$

where r_0 is the initial jet radius, u_0 – the initial velocity of the ejecting jet.

Assuming that the initial jet has an approximate same jet radius:

$$u_0 \propto Q_0 \tag{24}$$

Due to a tremendously high ejecting jet velocity, an extremely short period is needed for the jet reaches the receptor. Though the velocity will decrease due to the air drag and viscous resistance during this extremely short spinning process, we can use its initial velocity as its spinning velocity:

$$u \propto u_0 \propto Q_0 \tag{25}$$

According to eq. (18), the critical radius becomes larger for Sample 4, as a result the obtained fiber has larger diameter than other three samples. Using the data listed in tab. 2:

$$\frac{(r_{cr})_4}{(r_{cr})_1} = \frac{(u_0)_4}{(u_0)_1} = \frac{(Q_0)_4}{(Q_0)_1} = \frac{1}{0.5} = 2 \tag{26}$$

while experimental result is 836/431 = 1.94, with an accuracy of 3%.

The Sample 4 has a higher concentration than that of Sample 1, that means solvents involved in the moving jet is less, which can be faster evaporated, as a result, unsmooth surface due to solvent evaporation is formed, as illustrated in fig. 3.

Conclusion

This paper gives a theoretical analysis of the mechanism of unsmooth surface of fibers by electrospinning, though there are many mathematical models in open literature to describe the spinning process, however, all models ignore solvent evaporation. A fast solvent evaporation or sudden solvent evaporation always result in unsmooth surface, which can remarkable increase surface energy. This paper chooses a bi-solvent system with low boiling point. Due to the high ejecting velocity from the Taylor cone, the surface pressure of the moving jet is low according to Bernoulli principle, this is not helpful for a fast solvent evaporation, therefore, a low voltage is much needed for producing unsmooth fibers by electrospinning. Another important factor is volatile solvent. In practical applications, multiple solvent system is always welcome to produce unsmooth fibers.

Acknowledgment

The work is supported by National Natural Science Foundation of China under grant No. 51463021 and 51802244, Priority Academic Program Development of Jiangsu Higher Education Institutions (PAPD).

References

[1] Yin, J., *et al*., Numerical Approach to High-throughput of Nanofibers by a Modified Bubble-Electrospinning, *Thermal Science*, *24* (2020), 4, pp. 2367-2375
[2] Ahmed, A.. Xu, L., Numerical Analysis of the Electrospinning Process for Fabrication of Composite Fibers, *Thermal Science*, *24* (2020), 4, pp. 2377-2383
[3] Li, F., *et al*., A Hierarchical Hybrid Electrode for Rapid Oxygen Reduction Reaction below 800 °C, *Thermal Science*, *24* (2020), 4, pp. 2455-2462
[4] Li, X. X., *et al*., Nanofibers Membrane for Detecting Heavy Metal Ions, *Thermal Science*, *24* (2020), 4, pp. 2463-2468
[5] Li, X. X., *et al*., The Effect of Sonic Vibration on Electrospun Fiber Mats, *Journal of Low Frequency Noise Vibration and Active Control*, *38*(2019), 3-4, pp. 1246-1251
[6] Zhao, J. H., *et al*., Needle's Vibration in Needle-Disk Electrospinning Process: Theoretical Model and Experimental Verification, *Journal of Low Frequency Noise Vibration and Active Contro*l, *38* (2019), 3-4, pp. 1338-1344
[7] Wu, Y. K., Liu, Y., Fractal-Like Multiple Jets in Electrospinning Process, *Thermal Science*, *24* (2020), 4, pp. 2499-2505
[8] He, J H. Advances in Bubble Electrospinning, *Recent Patents on Nanotechnology*, *13* (2019), 3, pp. 162 -163

[9] Fan, J., Shang, X., Fractal Heat Transfer in Wool Fiber Hierarchy, *Heat Transf Res*., *44* (2013), 5, pp. 399-407
[10] Fan, J., *et al*.. Fractal Calculus for Analysis of Wool Fiber: Mathematical Insight of Its Biomechanism, *Journal of Engineered Fibers and Fabrics*, *14* (2020), Aug., (2019),
[11] Wang, Q. L., *et al*., Fractal Calculus and Its Application Explanation of Biomechanism of Polar Hairs (Vol. 26, 1850086, 2018), *Fractals*, *27* (2019), 5, 1992001
[12] Wang, Q. L., *et al*., Fractal Calculus and Its Application Explanation of Biomechanism of Polar Hairs (Vol. 26, 1850086, 2018), Fractals, *26* (2018), 6, 1850086
[13] Liu, F. J., *et al*., Silkworm (Bombyx Mori) Cocoon *vs*. Wild Cocoon: Multi-Layer Structure and Performance Characterization, *Thermal Science*, *23* (2019), 4, pp. 2135-2142
[14] He, C. H., *et al*., Fangzhu: An Ancient Chinese Nanotechnology for Water Collection from Air: History, Mathematical Insight, Promises and Challenges, *Mathematical Methods in the Applied Sciences*, On-line firste, https://doi.org/10.1002/mma.6384, 2020
[15] Liu, Y. Q., *et al*., Air Permeability of Nanofiber Membrane with Hierarchical Structure, *Thermal Science*, *22* (2018), 4, June, pp. 1637-1643
[16] Yu, D. N., *et al*. Snail-Based Nanofibers, *Mater Lett*., *22*0 (2018), June, pp. 5-7
[17] Liu, Y. Q., *et al*., Fabrication of Beltlike Fibers by Electrospinning, *Polymers*, *10* (2018), 10, 1087
[18] Yao, X., He, J. H., On Fabrication of Nanoscale Non-Smooth Fibers with High Geometric Potential and Nanoparticle's Non-Linear Vibration, *Thermal Science*, *24* (2020), 4, pp. 2491-2497
[19] Yang, Z. P., *et al*., A Fractal Model for Pressure Drop through a Cigarette Filter, *Thermal Science*, *24* (2020), 4, pp. 2653-2659
[20] Xu, L. Y., *et al*., Detection of Cigarette Smoke Using a Fiber Membrane Filmed with Carbon Nanoparticles and a Fractal Current Law, *Thermal Science*, *24* (2020), 4, pp. 2469-2474
[21] Liu, P., He, J. H., Geometric Potential: An Explanation of Nanofiber's Wettability, *Thermal Science*, *22* (2018), 1A, pp. 33-38
[22] Peng, N. B., He, J. H., Insight into the Wetting Property of a Nanofiber Membrane by the Geometrical Potential, *Recent Patents on Nanotechnology*, *14* (2020), 1, pp. 64-70
[23] Yang, Z. P., *et al*., On the Eross-Section of Shaped Fibers in the Dry Spinning Process: Physical Explanation by the Geometric Potential Theory, *Results in Physics*, *14* (2019), Sept., 102347
[24] Tian, D., *et al*., Geometrical Potential and Nanofiber Membrane's Highly Selective Adsorption Property, *Adsorption Science and Technology*, *37* (2019), 5-6, pp.
[25] Li, X. X., He, J. H., Nanoscale Adhesion and Attachment Oscillation under the Geometric Potential, – Part 1: The Formation Mechanism of Nanofiber Membrane in the Electrospinning, *Results in Physics*, *12* (2019), Mar., pp. 1405-1410
[26] Zhou, C. J., *et al*., What Factors Affect Lotus Effect, *Thermal Science*, *22* (2018), 4, pp. 1737-1743
[27] Wang, C. X., *et al*., Smart Adhesion by Surface Treatment: Experimental and Theoretical Insights, *Thermal Science*, *23* (2019), 4, pp. 2355-2363
[28] Fan, J., *et al*., Explanation of the Cell Orientation in a Nanofiber Membrane by the Geometric Potential Theory, *Results in Physics*, *15* (2019), Dec., 102537
[29] Jin, X., *et al*., Low Frequency of a Deforming Capillary Vibration – Part 1: Mathematical Model, *Journal of Low Frequency Noise Vibration and Active Control*, *38* (2019), 3-4, pp. 1676-1680
[30] He, J. H., Thermal Science for the Real World: *Reality and Challenge*, *Thermal Science*, 24 (2020), 4, pp. 2289-2294
[31] Tian, D., *et al*., Hall-Petch Effect and Inverse Hall-Petch Effect: A Fractal Unification, *Fractals*, *26* (2018), 6, 1850083
[32] Zhu, X., Xu, W., Effect of Surface Tension on the Behavior of Adhesive Contact Based on Lennard-Jones Potential Law, J. Mech. Phys. Solids, *111* (2018), Feb., pp. 170-183
[33] He, J. H., *et al*., Nanoeffects, Quantum-Like, Properties in Electrospun Nanofibers, *Chaos, Solitons and Fractals*, *33* (2007), 1, pp. 26-37
[34] He, J.BH., Liu, Y. P., Bubble Electrospinning: Patents, Promises and Challenges, *Recent Patents on Nanotechnology*, *14* (2020), 1, pp. 3-4
[35] He, C. H., *et al*., Taylor Series Solution for Fractal Bratu-Type Equation Arising in Electrospinning Process, *Fractals*, *28* (2020), 1, 2050011
[36] He, J. H., On the Height of Taylor Cone in Electrospinning, *Results in Physics*, *17* (2020), June, 103096

Paper submitted: December 1, 2019
Paper revised: June 20, 2020
Paper accepted: June 20, 2020